

Article

Structural, Mechanical, and Piezoelectric Properties of Janus Bidimensional Monolayers

Abdulrahman Mallah ¹, Mourad Debbichi ², Mohamed Houcine Dhaou ^{3,*} and Bilel Bellakhdhar ⁴¹ Department of Chemistry, College of Science, Qassim University, Buraydah 51452, Almolaydah, Saudi Arabia² Laboratoire de la Matière Condensée et Nanosciences, Département de Physique, Faculté des Sciences de Monastir, Monastir 5019, Tunisia³ Department of Physics, College of Science, Qassim University, Buraydah 51452, Almolaydah, Saudi Arabia⁴ Jeddah College of Technology, Jeddah 17608, Saudi Arabia

* Correspondence: m.dhaou@qu.edu.sa

Abstract: In the present work, the noncentrosymmetric 2D ternary Janus monolayers $Al_2XX'(X/X' = S, Se, Te \text{ and } O)$, $Si_2XX'(X/X' = P, As, Sb \text{ and } Bi)$, and $A_2PAs(A = Ge, Sn \text{ and } Pb)$ have been studied based on first-principles calculations. We find that all the monolayers exhibit in-plane d_{12} , and out-of-plane d_{13} piezoelectric coefficients due to the lack of reflection symmetry with respect to the central A atoms. Moreover, our calculations show that $Al_2OX(T = S, Se, Te)$ chalcogenide monolayers have higher absolute in-plane piezoelectric coefficients. However, the highest out-of-plane values are achieved in the Si_2PBi monolayer, larger than those of some advanced piezoelectric materials, making them very promising transducer materials for lightweight and high-performance piezoelectric nanodevices.

Keywords: first-principles; elastic; piezoelectric; 2D material, Janus monolayer



Citation: Mallah, A.; Debbichi, M.; Dhaou, M.H.; Bellakhdhar, B. Structural, Mechanical, and Piezoelectric Properties of Janus Bidimensional Monolayers. *Crystals* **2023**, *13*, 126. <https://doi.org/10.3390/cryst13010126>

Academic Editors: Alexei A. Bokov, Khitouni Mohamed and Joan-Josep Suñol

Received: 25 December 2022

Revised: 3 January 2023

Accepted: 6 January 2023

Published: 10 January 2023



Copyright: © 2023 by the authors. Licensee MDPI, Basel, Switzerland. This article is an open access article distributed under the terms and conditions of the Creative Commons Attribution (CC BY) license (<https://creativecommons.org/licenses/by/4.0/>).

1. Introduction

During the last 10 years, the study of two-dimensional (2D) materials has received a lot of attention as a result of the successful exfoliation of a graphene monolayer and the revealing of its special properties [1–3]. This class of materials can have significantly different, and sometimes unexpected properties compared to their bulk counterparts [4,5].

Among these, the Janus materials, which are characterized by two faces with two different local environment, have received rapidly increasing attention in recent years [6–9]. This new type of 2D material is successfully predicted by using first-principles calculations and is exfoliated mechanically from its bulk. The Janus-type two-dimensional (2D) monolayers have been studied extensively both experimentally and theoretically. They have many new physical properties that are not present in bulk structures or other conventional 2D materials. They also possess many exceptional physical properties, making them good candidates for many fields like electronics, optoelectronics, and catalysis. For instance, the potential of these stable 2D In_2X_2X' (X and $X' = S, Se, \text{ and } Te$) for photocatalytic and piezoelectric applications have been predicted by first-principles calculations [10]. Tuan et al. have predicted by first-principles calculations a novel stable Janus group III chalcogenide monolayers Al_2XY_2 ($X/Y = S, Se, Te$) suitable for applications in high-performance electronic nanodevices [8]. It has also been demonstrated by using first-principles calculations that the Janus Si_2XY ($X, Y = P, As, Sb, Bi$) monolayers have the potential for applications in spintronic devices [11]. Very recently, Yungang et al. [9] demonstrated that Nb_3SBr_7 and Ta_3SBr_7 bilayers are promising photocatalysts for water splitting due to their experimental feasibility and their distinct characteristic such as robust coexistence of intrinsic charge separations, ultrahigh solar-to-hydrogen (STH) efficiencies, and strong absorptions.

Piezoelectricity is a particularly interesting and useful property that has attracted tremendous interest because it allows for energy conversion between electrical and mechanical energy or vice versa. The growing demands for nanoscale and diverse functional

piezoelectric devices have oriented researchers to explore low-dimensional piezoelectric materials. However, the piezoelectric effect is an electromechanical interaction between stresses and strains, and polarizations and electric fields in noncentrosymmetric semiconductors and insulators [12–14]. It has been revealed that the lack of mirror symmetry in Janus structures has resulted in many new physical effects that are not present in symmetric structures such as the piezoelectric effect. This class of piezoelectric materials has numerous promising applications in sensors, transducers, actuators, active flexible electronics, and energy conversion devices [15,16]. As shown by Yonghu et al. [17] the coupling of topology and piezoelectricity in Janus MTeS (M = Ga and In) monolayers may offer a new platform for novel spintronic and piezotronic device applications. Additionally, the monolayer Fe₂IX (X = Cl and Br) becomes a viable platform for multifunctional spintronic applications with a large gap and high Curie temperature, due to the combination of piezoelectricity, topology, and the ferromagnetic ordering [18]. Furthermore, the coexistence of piezoelectricity and magnetism and their interaction in 2D materials can be utilized for making piezoelectric-based multifunctional nanodevices [19,20]. Despite the existence of many works about piezoelectricity properties based on binary 2D materials, few works are down for 2D ternary. However, the search for new materials with large piezoelectric coefficients remains a challenge for nanogenerators, ultrasensitive mechanical detectors, and consumer touch-sensor applications. Here, by using the density-functional perturbation theory, we have predicted the piezoelectric coefficients of some stable Janus monolayers, including Al₂XX'(X/X'=S, Se, Te and O), Si₂XX'(X/X'=P, As, Sb and Bi) and A₂PAs(A=Ge, Sn and Pb). These Janus monolayers are distinguished by the lack of mirror symmetry. We find that all the monolayers exhibit an in-plane d₁₂ and out-of plane d₁₃ piezoelectric coefficients. Our first-principles calculations show Al₂OX(T = S, Se, Te) chalcogenide monolayers have larger absolute in-plane piezoelectric coefficients. However, the highest out-of-plane value is achieved in the Si₂PBi monolayer, higher than those of some advanced piezoelectric materials.

2. Computational Details and Methods

Our DFT calculations are performed by using the Vienna ab initio simulation package (VASP) [21] and the projector-augmented wave method (PAW) with a cutoff energy of 600 eV. For the exchange-correlation potential, the generalized gradient approximation (GGA) within the Perdew–Burke–Ernzerhof (PBE) formalism is employed [22]. The Brillouin zone integration is sampled by using a Γ -centered $16 \times 16 \times 1$ k -point grid. For the all Janus A₂XX' monolayers, a vacuum spacing higher than 20 Å along the the direction perpendicular to the plane is included to avoid interactions between two neighboring images.

Elastic stiffness was calculated, including ionic relaxations by using the finite differences method [23]. However, the piezoelectric stress coefficients were calculated by employing the density functional perturbation theory (DFPT) method [23]. For more accurate results, a dense k -point mesh $25 \times 25 \times 1$ is used. All the structures are fully relaxed by using 10^{-6} eV and 10^{-3} eV/Å as convergence criteria for total energy and Hellmann–Feynman force, respectively. The localization of electrons in one unit cell with one monolayer is estimated by using the electron localization function (ELF) analysis, which was introduced in quantum chemistry to identify regions of space that can be associated with electron pairs [24].

3. Results and Discussion

3.1. Crystal Structures and Symmetry

In this paper, 15 possible models of A₂XX' monolayer, including Al₂XX'(X/X' = S, Se, Te and O), Si₂XX'(X/X' = P, As, Sb and Bi) and A₂PAs(A = Ge, Sn and Pb) are modeled. Figure 1 shows the top and side views of the optimized lattice structure of the Janus A₂XX' monolayers. The unit cell has a hexagonal symmetry with a C_{3v} space group, and are made up of one X atom, one X' atom, and two A atoms layers sandwiched between X and X'

atomic layers in the sequence X-A-A-X'. The absence of inversion symmetry distinguishes these monolayers from their parent binary structure.

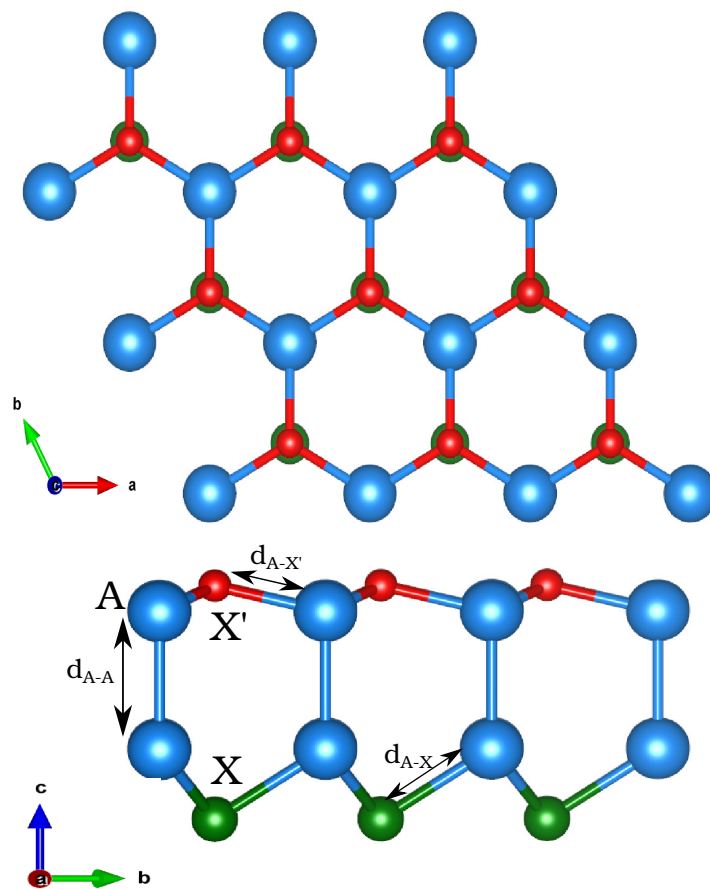


Figure 1. Top and side views of the prototype structure of the A₂XX' monolayers.

It was proven by previous theoretical works [11,25–28] based on static energy, phonon spectrum, and ab initio molecular dynamics simulations that all the Al₂XX' monolayers have thermal and kinetic stability. Meanwhile, DFT calculations that use different exchange-correlation functionals, such as PBE and HSE06, have been used to report the band structures of these monolayers. The calculated structural parameters of Al₂XX' monolayers are listed in Table 1. The obtained results are in good agreement with the available data [11,25–27].

Table 1. The lattice constant (a), A-A (d_{A-A}), A-X (d_{A-X}), A-X' $d_{A-X'}$ bond lengths and the work function difference $\Delta\Phi$ of 15 different structures of A_2XX' monolayers.

Monolayer	a (Å)	d_{A-A} (Å)	d_{A-X} (Å)	$d_{A-X'}$ (Å)	$\Delta\Phi$ (eV)
Al ₂ SO	3.36	2.60	2.26	2.00	0.30
Al ₂ SeO	3.42	2.59	2.38	2.03	0.42
Al ₂ TeO	3.49	2.63	2.61	2.06	0.24
Al ₂ TeS	3.85	2.58	2.41	2.63	0.16
Al ₂ TeSe	3.96	2.57	2.53	2.65	0.59
Al ₂ SeS	3.67	2.60	2.44	2.35	0.06
Si ₂ PAs	3.62	2.37	2.37	2.31	0.47
Si ₂ PSb	3.76	2.36	2.54	2.36	0.57
Si ₂ PBi	3.81	2.34	2.63	2.38	0.39
Si ₂ AsSb	3.84	2.34	2.57	2.45	0.26
Si ₂ AsBi	3.92	2.34	2.65	2.49	0.79
Si ₂ SbBi	4.08	2.35	2.69	2.64	0.26
Ge ₂ PAs	3.73	2.50	2.45	2.39	0.29
Sn ₂ PAs	4.03	2.90	2.59	2.65	0.087
Pb ₂ PAs	4.18	3.04	2.68	2.74	0.270

3.2. Elastic Theory and Properties

According to the symmetry group of our 2D compounds, only four elastic constants are nonzero, C_{11} , C_{22} , C_{12} , and C_{66} . Due to the symmetry of structures, we have $C_{11} = C_{22}$ et $C_{66} = \frac{1}{2}(C_{11}-C_{12})$. The calculated elastic constants C_{ij} are listed in Table 2. By checking the Born–Huang stability criteria [25]: $C_{11} > C_{12}$, $C_{22} > 0$, $C_{66} > 0$, and $C_{11}^2 - C_{21}^2 > 0$, we show that all the monolayers satisfy the stability condition.

Table 2. The 2D elastic constants C_{ij} (N/m), Young modulus Y^{2D} (N/m), Poisson ratio ν^{2D} , Shear modulus G^{2D} (N/m), and layer modulus γ^{2D} (N/m) of the Janus monolayers A_2XX' .

Monolayer	C_{11}	C_{12}	C_{66}	Y^{2D}	ν^{2D}	G^{2D}	γ^{2D}
Al ₂ SO	96.54	24.68	35.92	90.23	0.25	35.92	60.61
Al ₂ SeO	84.45	26.80	28.82	75.94	0.31	28.82	55.62
Al ₂ TeO	47.24	15.85	15.69	41.92	0.33	15.69	31.55
Al ₂ TeS	65.77	13.01	26.37	63.19	0.19	26.37	39.39
Al ₂ TeSe	62.20	13.23	24.48	59.38	0.21	24.48	37.72
Al ₂ SeS	75.50	15.58	29.96	72.29	0.20	29.96	45.54
Si ₂ PAs	112.95	16.96	47.99	110.40	0.15	47.99	64.95
Si ₂ PSb	94.02	13.96	40.03	91.95	0.14	40.03	53.99
Si ₂ PBi	52.36	24.72	13.82	40.69	0.47	13.82	38.54
Si ₂ AsSb	88.94	16.01	36.46	86.05	0.18	36.46	52.48
Si ₂ AsBi	80.65	18.74	30.95	76.30	0.23	30.95	49.70
Si ₂ SbBi	70.54	15.95	27.29	66.93	0.22	27.29	43.24
Ge ₂ PAs	98.80	20.54	39.12	94.52	0.20	39.12	59.67
Sn ₂ PAs	73.34	17.80	27.77	69.02	0.24	27.77	45.57
Pb ₂ PAs	44.19	6.57	18.80	43.21	0.14	18.80	25.38

The elastic properties of the A_2XX' monolayers are examined in terms of the in-plane Young modulus and the Poisson ratios. Due to hexagonal symmetry, A_2XX' monolayers are mechanically isotropic.

In terms of these elastic constants, the layer modulus is

$$\gamma^{2D} = \frac{1}{2}(C_{11} + C_{12}). \quad (1)$$

The angular dependence of the in-plane Poisson's ratio ($\nu^{2D}(\theta)$) and Young's modulus ($Y^{2D}(\theta)$) are obtained from the following formulas [1]:

$$\nu^{2D}(\theta) = \frac{C_{12}S^4 - BS^2C^2 + C_{12}C^4}{C_{11}S^4 + AS^2C^2 + C_{22}C^4} \quad (2)$$

$$Y^{2D}(\theta) = \frac{C_{11}C_{22} - C_{12}^2}{C_{11}S^4 + AS^2C^2 + C_{22}C^4} \quad (3)$$

where $S = \sin(\theta)$, $C = \cos(\theta)$, $A = \frac{C_{11}C_{22} - C_{12}^2}{C_{66}} - 2C_{12}$ and $B = C_{11} + C_{12} - \frac{C_{11}C_{22} - C_{12}^2}{C_{66}}$.

The orientation-dependent values for the all monolayers reveal strong isotropy of Young's modulus as well as Poisson's ratio. As an example, we show in Figure 2 the angular dependence of the Poisson's ratio (a) and Young's modulus of Al_2SSe monolayer. We find that ν^{2D} and Y^{2D} plots are perfect circles, implying that these monolayers have highly isotropic elasticity due to their 2D isotropic atomic structures. The corresponding computed values are listed in Table 2. For the all monolayers, our calculated values of the elastic stiffness are in concordance with the available data [11,25,26]. The Young's moduli values are obviously smaller than those of other well-known 2D materials, such as graphene, hexagonal boron nitride layer and MoS_2 [29–31], demonstrating their mechanical flexibility and can resist significantly to the mechanical strain. The calculated ν^{2D} values of all the monolayers except Si_2PBi are less than 0.33, which implies that these monolayers are brittle based on the Frantsevich rule [32,33].

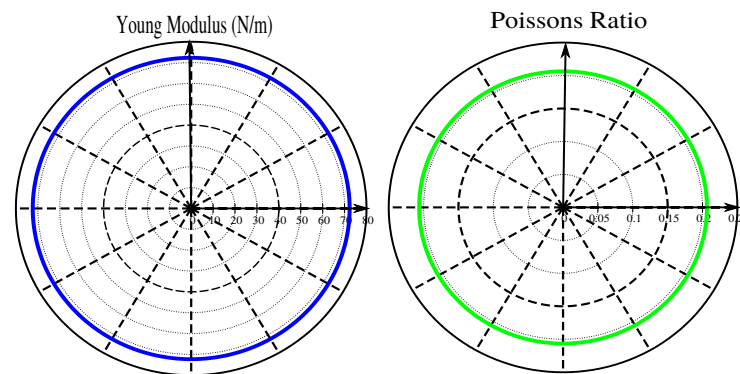


Figure 2. Orientation dependence on the in-plane Poisson's ratio (ν^{2D}) and Young's modulus (Y^{2D}) of Al_2SSe monolayer.

3.3. Piezoelectric Properties

In $\text{A}_2\text{XX}'$, the difference in atom size and electronegativity, as well as the different bond types between Al-X ($d_{\text{A-X}}$) and Al-X' ($d_{\text{A-X}'}$) all contribute to unequal charge distributions in the systems as shown in the inset of the Figure 3, resulting in noncentrosymmetric materials. As an example, the planar average of the electrostatic potential energy of Al_2SSe is shown in Figure 3. As can clearly be seen, a significant potential difference between the two sides of the monolayer, reflecting the formation of an internal electric field and surface work function difference ($\Delta\Phi$). For the other compounds, the planar average of the electrostatic potential energy is calculated and the extracted work function difference is regrouped in Table 1, which is proportional to the magnitude of the dipole moment according to the Helmholtz equation [34].

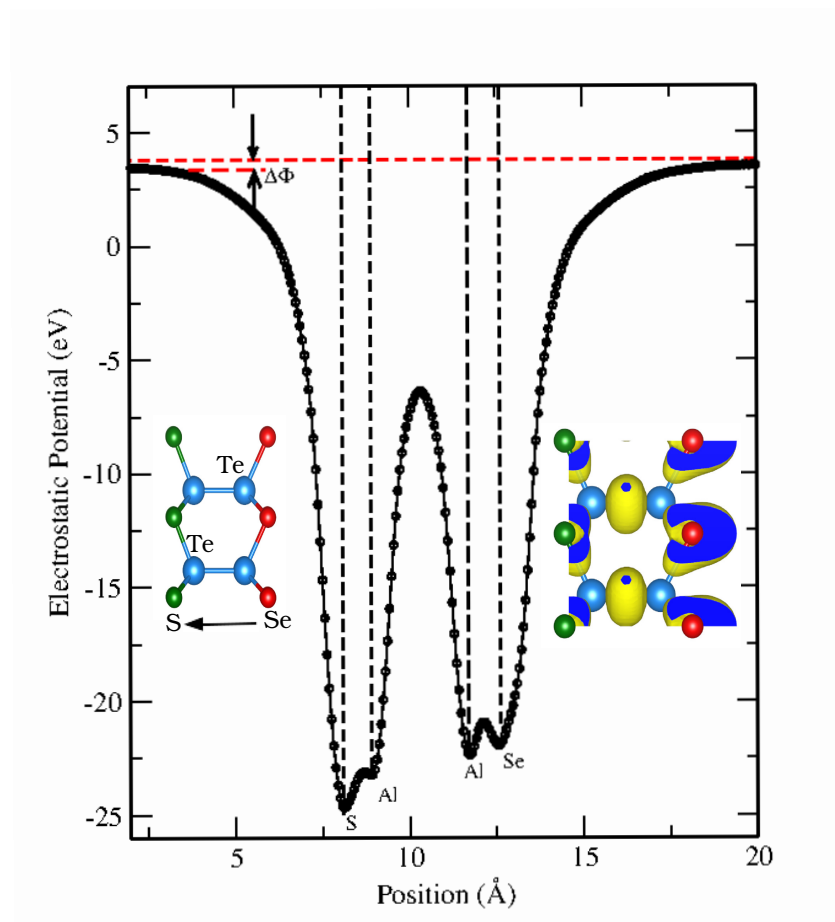


Figure 3. Planar average of the electrostatic potential energy for the Al_2SSe . In the inset, the electron localization function (ELF) of the Al_2SSe . The arrow indicates the direction of the local electric field.

The aforementioned properties, such as the lack of inversion symmetry and the intrinsic polar electric field, are two possible causes for the emergence of piezoelectricity in the materials. The relaxed-ion third-rank piezoelectric tensors e_{ijk} and d_{ijk} , which are the sum of ionic and electronic contributions, can be evaluated by

$$e_{ijk} = e_{ijk}^{\text{ion}} + e_{ijk}^{\text{elc}} = \frac{\partial P_i}{\partial \varepsilon_{ij}} \quad (4)$$

and

$$d_{ijk} = d_{ijk}^{\text{ion}} + d_{ijk}^{\text{elc}} = \frac{\partial P_i}{\partial \sigma_{ij}}, \quad (5)$$

where ε_{ij} , σ_{ij} and P_i represent the strain, stress, and polarization tensors, respectively. For 2D materials, $\varepsilon_{ij} = \sigma_{ij} = 0$ for $i = 3$ [16].

By using the Voigt notation, (1 = xx, 2 = yy, 3 = zz, 4 = yz, 5 = zx, and 6 = xy) [35]. The second-rank piezoelectric tensors e_{ij} and d_{jk} are related via the elastic stiffness tensor by

$$e_{ij} = d_{ik} C_{jk}. \quad (6)$$

For our Janus monolayers the point-group symmetry belongs to $3m$, and the nonzero piezoelectric stress tensors, e_{ij} are given as

$$e_{ij} = \begin{pmatrix} \cdot & \cdot & \cdot & \cdot & e_{15} & e_{12} \\ e_{12} & -e_{12} & \cdot & e_{15} & \cdot & \cdot \\ e_{31} & e_{31} & e_{31} & \cdot & \cdot & \cdot \end{pmatrix}.$$

For 2D materials $e_{ij}^{2D} = d_{ik}^{2D} C_{jk}$, where $M_{ij}^{2D} = M/l_z$, ($M = e$ or d), and l_z is the length of the unit cell along the z direction.

Based on Equation (6), the unique in-plane and out-of-plane piezoelectric coefficients e_{12}^{2D} , d_{12}^{2D} and e_{31}^{2D} , d_{31}^{2D} , respectively, are nonzero. The corresponding piezoelectric tensors matrix can be written as

$$\begin{pmatrix} 0 & 0 & e_{12}^{2D} \\ e_{12}^{2D} & -e_{12}^{2D} & 0 \\ e_{31}^{2D} & e_{31}^{2D} & 0 \end{pmatrix} = \begin{pmatrix} 0 & 0 & 2d_{12}^{2D} \\ d_{12}^{2D} & -d_{12}^{2D} & 0 \\ d_{31}^{2D} & d_{31}^{2D} & 0 \end{pmatrix} \times \begin{pmatrix} C_{11} & C_{12} & 0 \\ C_{12} & C_{11} & 0 \\ 0 & 0 & C_{66} \end{pmatrix}.$$

The d_{22} and d_{31} can be calculated by

$$d_{12}^{2D} = \frac{e_{12}^{2D}}{C_{11} - C_{22}} \quad (7)$$

and

$$d_{31}^{2D} = \frac{e_{31}^{2D}}{C_{11} + C_{22}}. \quad (8)$$

In the following, we use e_{ij} and d_{ij} instead of the e_{ij}^{2D} and d_{ij}^{2D} symbol, respectively. In this work, we adapted the relaxed-ion method, which is the sum of electronic and ionic parts to calculate the piezoelectric coefficients, which is the more reliable method compared to that of the clamped-ion one [36]. To verify the reliability of the applied method, we have first computed piezoelectric stress coefficient e_{11} for 1H-MoS₂ monolayer and found a predicted value as higher as $\sim 2.27 \times 10^{-10}$ C/m, in excellent agreement with the experimental value and the reported theoretical studies [12,37]. By using the above procedures, we derive the piezoelectric coefficients e_{ij} of the all monolayers. The results are shown in Figure 4. More significantly, these Janus monolayers with broken mirror symmetry possess, in addition to in-plane e_{12}/d_{12} nonzero out-of-plane piezoelectric coefficients e_{13}/d_{13} . The minus sign in calculated values indicates the direction of polarization.

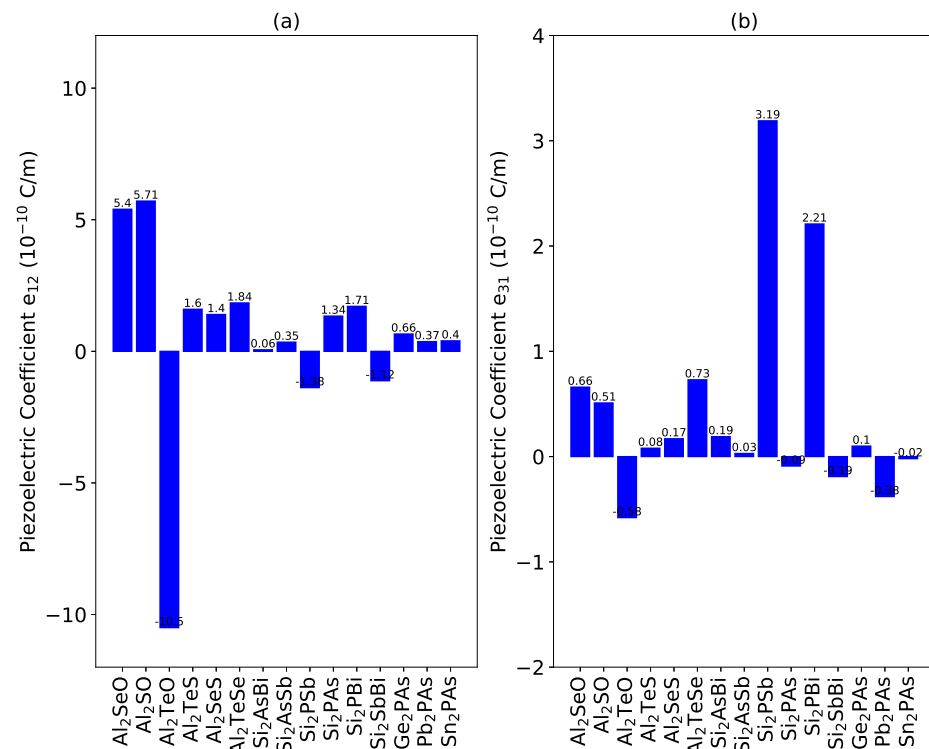


Figure 4. Piezoelectric coefficients (a) e_{12} and (b) e_{31} of 15 different structures of A_2XX' monolayers.

As shown in Figures 4a and 5a for a given metal element A, the monolayers containing heavier chalcogenide atoms (Te, Se and S) have the higher in-plane piezoelectric coefficient $|e_{12}|/|d_{12}|$ values. Compared with other 2D piezoelectric materials such as MoX_2 ($X = \text{S, Se, Te}$) and MoTO ($T = \text{S, Se, Te}$) with a value of 3.64–5.43 pm/V [30,38], the Janus Al_2OX ($T = \text{S, Se, Te}$) chalcogenide monolayers have larger absolute in-plane piezoelectric coefficients by several folds. More noticeably, $|d_{12}|$ attains 18.20 and 17.42 pm/V for Al_2TeO and Al_2SeO monolayers, respectively, in same order of magnitude as the Janus M_2SeX ($M = \text{Ge, Sn; X = S, Te}$) monolayers [13], which makes them appropriate for 2D piezoelectric sensors and nanogenerators. Some materials, such as the monolayers Al_2TeSe and Si_2PBi , have large d_{12} values but small e_{12} values because their Young's moduli are small, limiting the amount of force applied in electric field-induced deformations.

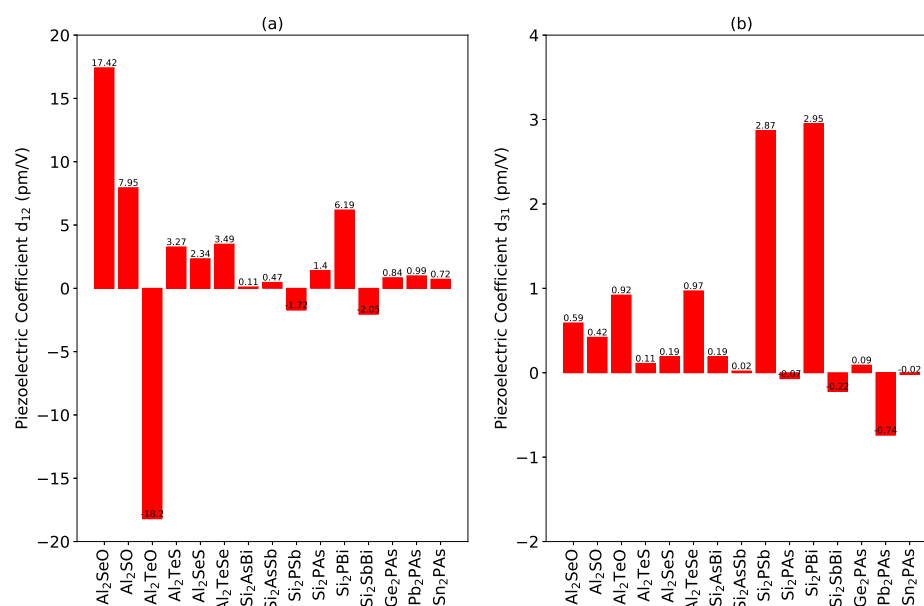


Figure 5. Piezoelectric coefficients (a) d_{12} and (b) d_{31} of 15 different structures of $\text{A}_2\text{XX}'$ monolayers.

The noncentrosymmetric crystal structure of the $\text{A}_2\text{XX}'$ monolayers in the out-of-plane direction gives rise to the finite out-of-plane piezoelectric constant. For all the monolayers presented in this work, the value of the out-of-plane strain piezoelectric coefficient d_{31} (Figure 5b) is about two orders of magnitude lower than the in-plane coefficient d_{12} . This means that vertical piezoelectric polarization due to vertical strain is much stronger than that of the in-plane strain. But these values are still comparable to other 2D materials such as Te_2Se , MoSte , In_2SSe , $\text{TiNX}_{0.5}\text{Y}_{0.5}$ ($X, Y = \text{Cl, Br, F}$) and 1T-MX_2 ($M = \text{Zr and Hf; X = S, Se, and Te}$) [16,39,40]. The highest d_{31} value (2.95 pm/V) is achieved in the Si_2PBi and Si_2PSb monolayers, higher to those of some advanced piezoelectric materials such as MoSte , GaN wurtzite , $\text{M}_2\text{XX}'$ ($M = \text{Ga, In; X, X}' = \text{S, Se, Te and X} \neq \text{X}'$) and $\text{MM}'\text{X}_2$ ($M, M' = \text{Ga, In and M}' \neq \text{M; X = S, Se, Te}$) [16,36]. This value is also comparable to that of the Janus Te_2Se multilayers with antiparallel orientations, $\text{CrF}_{1.5}\text{I}_{1.5}$, $\text{Sb}_2\text{Te}_2\text{Se}$, $\text{Sb}_2\text{Se}_2\text{Te}$, TePtS and TePtSe [14,16,41,42]. This significant out-of-plane piezoelectric effect would give these Janus monolayers a variety of functions in piezoelectric applications.

By comparing the d_{31} of the six 2D Janus $\text{Si}_2\text{XX}'$ monolayers, we conclude that the absolute value of the out-of-plane piezoelectric coefficient d_{31} increases with the electronegativity difference between the atoms on both sides of the monolayer, X and X'. This finding is also valid for the $\text{Al}_2\text{XX}'$ monolayers. This is understandable given that the difference in atomic sizes of X and X' breaks the reflection symmetry along the vertical direction, resulting in vertical piezoelectric polarization, which becomes stronger when the electronegativity difference between atoms increases.

4. Conclusions

On the basis of first-principles calculations, we have systematically studied the piezoelectric properties of some Janus 2D monolayers, Al_2XX' ($X/X' = S, Se, Te$ and O), Si_2XX' ($X/X' = P, As, Sb$ and Bi) and A_2PAs ($A = Ge, Sn$ and Pb). The absence of inversion symmetry in these Janus structures gives rise to in-plane and out-of-plane piezoelectric coefficients. Our calculations, by using the DFPT method, reveal that the monolayers containing heavier chalcogenide atoms (Te, Se and S) have a higher in-plane piezoelectric coefficient larger than those of the widely studied $1H-MoX_2$ ($X = S, Se, Te$) monolayers. Moreover, all the monolayers are characterized by out-of-plane piezoelectric coefficients e_{31}/d_{31} , due to the lack of reflection symmetry with respect to the central A atoms. The highest values of d_{31} (~ 2.9 pm/V) are achieved for the Si_2PBi and S_2PSb monolayers due to their mechanical flexibility.

Author Contributions: Conceptualization: A.M., M.D., M.H.D. and B.B.; Data curation: A.M., M.D. and M.H.D.; Formal analysis: M.D., M.H.D. and B.B.; Funding acquisition: A.M. and M.H.D.; Investigation: A.M. and M.D.; Resources: M.D.; Validation: A.M. and M.D.; Writing-original draft: A.M., M.D. and M.H.D. All authors have read and agreed to the published version of the manuscript.

Funding: Qassim University, represented by the Deanship of Scientific Research, on the material support for this research under the number (10244-cos-2020-1-3-I).

Data Availability Statement: Data can be requested from the authors.

Acknowledgments: The authors gratefully acknowledge Qassim University, represented by the Deanship of Scientific Research, on the material support for this research under the number (10244-cos-2020-1-3-I) during the academic year 1442AH/2020AD.

Conflicts of Interest: On behalf of all authors, the corresponding author states that there is no conflict of interest.

References

1. Debbichi, M.; Alhodaib, A. Stability, electronic and magnetic properties of the penta-CoAsSe monolayer: A first-principles and Monte Carlo study. *Phys. Chem. Chem. Phys.* **2022**, *24*, 5680. [[CrossRef](#)] [[PubMed](#)]
2. Debbichi, M.; Mallah, A.; Dhaou, M.H.; Lebègue, S. First-Principles Study of Monolayer penta-CoS₂ as a Promising Anode Material for Li/Na-ion Batteries. *Phys. Rev. Appl.* **2021**, *16*, 024016. [[CrossRef](#)]
3. Debbichi, M.; Said, H.; Garbouj, H.; El Hog, S.; An Dinh, V. A new ternary Pentagonal Monolayer based on Bi with large intrinsic Dzyaloshinskii-Moriya interaction. *J. Phys. D Appl. Phys.* **2021**, *55*, 015002. [[CrossRef](#)]
4. Debbichi, M.; Debbichi, L.; Lebègue, S. Tuning the magnetic and electronic properties of monolayer chromium tritelluride through strain engineering. *Phys. Lett. A* **2020**, *384*, 126684. [[CrossRef](#)]
5. Debbichi, M.; Debbichi, L.; Lebègue, S. Controlling the stability and the electronic structure of transition metal dichalcogenide single layer under chemical doping. *Phys. Lett. A* **2019**, *383*, 2922–2927. [[CrossRef](#)]
6. Sa, B.; Hu, R.; Zheng, Z.; Xiong, R.; Zhang, Y.; Wen, C.; Zhou, J.; Sun, Z. High-Throughput Computational Screening and Machine Learning Modeling of Janus 2D III–VI van der Waals Heterostructures for Solar Energy Applications. *Chem. Mater.* **2022**, *34*, 6687–6701. [[CrossRef](#)]
7. Zhang, L.; Gu, Y.; Du, A. Two-Dimensional Janus Antimony Selenium Telluride with Large Rashba Spin Splitting and High Electron Mobility. *ACS Omega* **2021**, *6*, 31919–31925. [[CrossRef](#)]
8. Vu, T.V.; Hieu, N.N. Novel Janus group III chalcogenide monolayers Al_2XY_2 ($X/Y = S, Se, Te$): first-principles insight onto the structural, electronic, and transport properties. *J. Phys. Condens. Matter* **2021**, *34*, 115601. [[CrossRef](#)]
9. Zhou, Y.; Zhou, L.; He, J. 2D Nb_3SBr_7 and Ta_3SBr_7 : Experimentally Achievable Janus Photocatalysts with Robust Coexistence of Strong Optical Absorption, Intrinsic Charge Separation, and Ultrahigh Solar-to-Hydrogen Efficiency. *ACS Appl. Mater. Interfaces* **2022**, *14*, 1643–1651. [[CrossRef](#)]
10. Wang, P.; Liu, H.; Zong, Y.; Wen, H.; Xia, J.B.; Wu, H.B. Two-Dimensional In_2X_2X' (X and $X' = S, Se, Te$) Monolayers with an Intrinsic Electric Field for High-Performance Photocatalytic and Piezoelectric Applications. *ACS Appl. Mater. Interfaces* **2021**, *13*, 34178–34187. [[CrossRef](#)]
11. Babaee Touski, S.; Ghobadi, N. Structural, electrical, and Rashba properties of monolayer Janus Si_2XY ($X, Y = P, As, Sb, Bi$). *Phys. Rev. B* **2021**, *103*, 165404. [[CrossRef](#)]
12. Blonsky, M.N.; Zhuang, H.L.; Singh, A.K.; Hennig, R.G. Ab Initio Prediction of Piezoelectricity in Two-Dimensional Materials. *ACS Nano* **2015**, *9*, 9885–9891. [[CrossRef](#)] [[PubMed](#)]

13. Qiu, J.; Zhang, F.; Li, H.; Chen, X.; Zhu, B.; Guo, H.; Ding, Z.; Bao, J.; Yu, J. Giant Piezoelectricity of Janus M_2SeX ($M = Ge, Sn; X = S, Te$) Monolayers. *IEEE Electron Device Lett.* **2021**, *42*, 561–564. [[CrossRef](#)]
14. Guo, S.D.; Guo, X.S.; Cai, X.X.; Mu, W.Q.; Ren, W.C. Intrinsic piezoelectric ferromagnetism with large out-of-plane piezoelectric response in Janus monolayer $CrBr_{1.5}I_{0.5}$. *J. Appl. Phys.* **2021**, *129*, 214301. [[CrossRef](#)]
15. Wu, W.; Wang, Z.L. Piezotronics and piezo-phototronics for adaptive electronics and optoelectronics). *Nat. Rev. Mater.* **2016**, *1*, 16031. [[CrossRef](#)]
16. Chen, Y.; Liu, J.; Yu, J.; Guo, Y.; Sun, Q. Symmetry-breaking induced large piezoelectricity in Janus tellurene materials. *Phys. Chem. Chem. Phys.* **2019**, *21*, 1207–1216. [[CrossRef](#)] [[PubMed](#)]
17. Wang, Y.; Lei, S.; Huang, Q.; Wan, N.; Xu, F.; Yu, H.; Li, C.; Chen, J. Coexistence of the Piezoelectricity and Intrinsic Quantum-Spin Hall Effect in GaTeS and InTeS Monolayers: Implications for Spintronic Devices. *ACS Appl. Nano Mater.* **2022**, *5*, 11037–11044. [[CrossRef](#)]
18. Guo, S.D.; Mu, W.Q.; Xiao, X.B.; Liu, B.G. Intrinsic room-temperature piezoelectric quantum anomalous hall insulator in Janus monolayer Fe_2IX ($X = Cl$ and Br). *Nanoscale* **2021**, *13*, 12956–12965. [[CrossRef](#)] [[PubMed](#)]
19. Guo, S.D.; Zhu, Y.T.; Qin, K.; Ang, Y.S. Large out-of-plane piezoelectric response in ferromagnetic monolayer NiClI. *Appl. Phys. Lett.* **2022**, *120*, 232403. [[CrossRef](#)]
20. Noor-A-Alam, M.; Nolan, M. Large piezoelectric response in ferroelectric/multiferroelectric metal oxyhalide MOX_2 ($M = Ti, V$ and $X = F, Cl$ and Br) monolayers. *Nanoscale* **2022**, *14*, 11676–11683. [[CrossRef](#)]
21. Kresse, G.; Hafner, J. Ab initio molecular dynamics for liquid metals. *Phys. Rev. B* **1993**, *47*, 558–561. [[CrossRef](#)] [[PubMed](#)]
22. Perdew, J.P.; Burke, K.; Ernzerhof, M. Generalized Gradient Approximation Made Simple. *Phys. Rev. Lett.* **1996**, *77*, 3865. [[CrossRef](#)] [[PubMed](#)]
23. Wu, X.; Vanderbilt, D.; Hamann, D.R. Systematic treatment of displacements, strains, and electric fields in density-functional perturbation theory. *Phys. Rev. B* **2005**, *72*, 035105. [[CrossRef](#)]
24. Becke, A.D.; Edgecombe, K.E. A simple measure of electron localization in atomic and molecular systems. *J. Chem. Phys.* **1990**, *92*, 5397–5403. [[CrossRef](#)]
25. Liu, M.Y.; Gong, L.; He, Y.; Cao, C. Intraband Lifshitz transition and Stoner ferromagnetism in Janus PA_2As ($A=Si, Ge, Sn$, and Pb) monolayers. *Phys. Rev. B* **2021**, *104*, 035409. [[CrossRef](#)]
26. Demirtas, M.; Varjovi, M.J.; Cicek, M.M.; Durgun, E. Tuning structural and electronic properties of two-dimensional aluminum monochalcogenides: Prediction of Janus $Al_2XX'(X/X':O, S, Se, Te)$ monolayers. *Phys. Rev. Mater.* **2020**, *4*, 114003.
27. Kumar, V.; Jung, J. Two-dimensional Janus group-III ternary chalcogenide monolayer compounds B_2XY , Al_2XY , and $BAIX_2$ ($X, Y = S, Se, Te$) with high carrier mobilities. *Bull. Korean Chem. Soc.* **2022**, *43*, 138–146. [[CrossRef](#)]
28. Huang, A.; Shi, W.; Wang, Z. Optical Properties and Photocatalytic Applications of Two-Dimensional Janus Group-III Monochalcogenides. *J. Phys. Chem. C* **2019**, *123*, 11388–11396. [[CrossRef](#)]
29. Lee, C.; Wei, X.; Kysar, J.W.; Hone, J. Measurement of the Elastic Properties and Intrinsic Strength of Monolayer Graphene. *Science* **2008**, *321*, 385–388. [[CrossRef](#)]
30. Duerloo, K.A.N.; Ong, M.T.; Reed, E.J. Intrinsic Piezoelectricity in Two-Dimensional Materials. *J. Phys. Chem. Lett.* **2012**, *3*, 2871–2876.
31. Song, L.; Ci, L.; Lu, H.; Sorokin, P.B.; Jin, C.; Ni, J.; Kvashnin, A.G.; Kvashnin, D.G.; Lou, J.; Yakobson, B.I.; et al. Large Scale Growth and Characterization of Atomic Hexagonal Boron Nitride Layers. *Nano Lett.* **2010**, *10*, 3209–3215. [[CrossRef](#)] [[PubMed](#)]
32. Frantsevich, I.; Voronov, F.; Bokuta, S. *Elastic Constants and Elastic Moduli of Metals and Insulators Handbook*; Naukova Dumka: Kiev, Ukraine, 1983, pp. 60–180.
33. Debbichi, M.; Alresheedi, F. First-principles calculations of mechanical, electronic and optical properties of a new imidooxonitridophosphate. *Chem. Phys.* **2020**, *538*, 110917. [[CrossRef](#)]
34. Xiao, W.Z.; Xu, L.; Xiao, G.; Wang, L.L.; Dai, X.Y. Two-dimensional hexagonal chromium chalcogenides with large vertical piezoelectricity, high-temperature ferromagnetism, and high magnetic anisotropy. *Phys. Chem. Chem. Phys.* **2020**, *22*, 14503–14513. [[CrossRef](#)]
35. Yin, H.; Gao, J.; Zheng, G.P.; Wang, Y.; Ma, Y. Giant Piezoelectric Effects in Monolayer Group-V Binary Compounds with Honeycomb Phases: A First-Principles Prediction. *J. Phys. Chem. C* **2017**, *121*, 25576–25584. [[CrossRef](#)]
36. Guo, Y.; Zhou, S.; Bai, Y.; Zhao, J. Enhanced piezoelectric effect in Janus group-III chalcogenide monolayers. *Appl. Phys. Lett.* **2017**, *110*, 163102. [[CrossRef](#)]
37. Zhu, H.; Wang, Y.; Xiao, J.; Liu, M.; Xiong, S.; Wong, Z.J.; Ye, Z.; Yin, X.; Zhang, X. Observation of Piezoelectricity in Free-standing Monolayer Molybdenum Disulfide. *Nat. Nanotech.* **2015**, *10*, 151–155. [[CrossRef](#)]
38. Li, Y.Q.; Wang, X.Y.; Zhu, S.Y.; Tang, D.S.; He, Q.W.; Wang, X.C. Active Asymmetric Electron-Transfer Effect on the Enhanced Piezoelectricity in $MoTO$ ($T = S, Se, or Te$) Monolayers and Bilayers. *J. Phys. Chem. Lett.* **2022**, *13*, 9654–9663. [[CrossRef](#)]
39. Shi, X.; Yin, H.; Jiang, S.; Chen, W.; Zheng, G.P.; Ren, F.; Wang, B.; Zhao, G.; Liu, B. Janus 2D titanium nitride halide $TiNX_{0.5}Y_{0.5}$ ($X, Y = F, Cl, or Br$ and $X \neq Y$) monolayers with giant out-of-plane piezoelectricity and high carrier mobility. *Phys. Chem. Chem. Phys.* **2021**, *23*, 3637. [[CrossRef](#)]
40. Jena, N.; Rawat, A.; Ahammed, R.; Mohanta, M.K.; De Sarkar, A. Emergence of high piezoelectricity along with robust electron mobility in Janus structures in semiconducting Group IVB dichalcogenide monolayers. *J. Mater. Chem. A* **2018**, *6*, 24885.

41. Qiu, J.; Li, H.; Chen, X.; Zhu, B.; Guo, H.; Zhang, F.; Ding, Z.; Lang, L.; Yu, J.; Bao, J. Piezoelectricity of Janus Sb₂Se₂Te monolayers: A first-principles study. *J. Appl. Phys.* **2021**, *129*, 125109. [[CrossRef](#)]
42. Kahraman, Z.; Kandemir, A.; Yagmurcukardes, M.; Sahin, H. Single-Layer Janus-Type Platinum Dichalcogenides and Their Heterostructures. *J. Phys. Chem. C* **2019**, *123*, 4549–4557. [[CrossRef](#)]

Disclaimer/Publisher's Note: The statements, opinions and data contained in all publications are solely those of the individual author(s) and contributor(s) and not of MDPI and/or the editor(s). MDPI and/or the editor(s) disclaim responsibility for any injury to people or property resulting from any ideas, methods, instructions or products referred to in the content.